Electronic Supporting Information

for

The role of structural defects in the fluoride-mediated synthesis of aluminosilicate zeolites

Kingsley Christian Kemp,[a] Ömer F. Altundal,[b] Donghui Jo,[c] Weidong Huang,[d,e] Qiang Wang,[d,e] Feng Deng,[d,e] German Sastre*[b] and Suk Bong Hong*[a]

[a] Center for Ordered Nanoporous Materials Synthesis, Division of Environmental Science and Engineering, POSTECH, Pohang 37673, Korea.

[b] Instituto de Tecnologia Quimica (UPV-CSIC), Universidad Politécnica de Valencia, Avenida Naranjos s/n, Valencia 46022, Spain.

[c] Low-Carbon Petrochemical Research Center, Korea Research Institute of Chemical Technology, Daejeon 34114, Korea.

[d] State Key Laboratory of Magnetic Resonance and Atomic and Molecular Physics, National Center for Magnetic Resonance in Wuhan, Innovation Academy for Precision Measurement Science and Technology, Chinese Academy of Sciences, Wuhan 430071, P. R. China.

[e] University of Chinese Academy of Sciences, Beijing 100049, P. R. China.

Contents

S1. Experimental

S1.1. Organic structure-directing agents (OSDAs) preparation S3

S1.2. Zeolite Synthesis S4

S1.3. Characterization S4

S2. Computational Models and Methods

S2.1. Models: Unit cells considered S6

S2.2. Calculations for pure-silica zeolites S6

S2.3. Calculations for aluminosilicate zeolites (with/without fluorides and defects) S7

S2.4. Synthesis energy calculations S8

S2.5. Force field used S11

Tables S1-S21 S13-S33

Figs. S1 – S12 S34-S45

References S46-S47

S1. Experimental

S1.1. Organic structure-directing agent (OSDAs) preparation

In a typical preparation of a series of trimethylpyridinium (TMP) isomers in their hydroxide form used as OSDAs in zeolite synthesis, a mixture of 0.10 mol of an appropriate dimethylpyridine and 0.3 mol of iodomethane (98%, Kanto) was stirred in 200 mL of acetone at 25 °C for 3 days.

1,2,3-Trimethylpyridinium (123TMP) iodide was obtained by reacting 2,3-dimethylpyridine (99%, Aldrich) with iodomethane (98%, Kanto). ^{1}H NMR (300 MHz, D_2O): δ 8.42, 8.14, 7.59, 4.15, 2.62, 2.42 ppm. ^{13}C NMR (75 MHz, D_2O): δ 147.3, 145.0, 140.5, 126.0, 48.3, 20.9, 18.3 ppm.

1,2,4-Trimethylpyridinium (124TMP) iodide was obtained by reacting 2,4-dimethylpyridine (>98%, TCI) with iodomethane (98%, Kanto). ^{1}H NMR (300 MHz, D_2O): δ 8.39, 7.64, 7.54, 4.07, 2.64, 2.48 ppm. ^{13}C NMR (75 MHz, D_2O): δ 159.1, 154.4, 144.4, 129.5, 125.8, 44.5 ppm.

1,2,5-Trimethylpyridinium (125TMP) iodide was obtained by reacting 2,5-dimethylpyridine (>98%, TCI) with iodomethane (98%, Kanto). ^{1}H NMR (300 MHz, D_2O): δ 8.45, 8.10, 7.67,4.09, 2.64, 2.37 ppm. ^{13}C NMR (75 MHz, D_2O): δ 147.7, 146.9, 138.4, 130.6, 47.2, 21.2, 18.9 ppm.

1,2,6-Trimethylpyridinium (126TMP) iodide was obtained by reacting 2,6-dimethylpyridine (99%, Thermo Scientific) with iodomethane (98%, Kanto). ^{1}H NMR (300 MHz, D_2O): δ 8.10, 7.65, 3.99, 2.72 ppm. ^{13}C NMR (75 MHz, D_2O): δ 155.8, 143.9, 127.1, 39.9, 21.1 ppm.

1,3,4-Trimethylpyridinium (134TMP) iodide was obtained by reacting 3,4-dimethylpyridine (98%, Aldrich) with iodomethane (98%, Kanto). ^{1}H NMR (300 MHz, D_2O): δ 8.37, 8.32, 7.66, 4.16, 2.44, 2.32 ppm. ^{13}C NMR (75 MHz, D_2O): δ 160.1, 145.1, 143.3, 140.1, 129.8,

48.9, 21.3, 17.9 ppm.

1,3,5-Trimethylpridinium (135TMP) iodide was obtained by reacting 3,5-dimethylpyridine (>98%, TCI) with iodomethane (98%, Kanto). ^{1}H NMR (300 MHz, D_2O): δ 8.38, 8.12, 4.23, 2.43 ppm. ^{13}C NMR (75 MHz, D_2O): δ 146.3, 141.8, 138.7, 47.7, 17.5 ppm.

The iodide salt of each cation obtained was washed with diethyl ether three times, dried at 80 °C, and then converted into the hydroxide form by anion exchange in aqueous solution using Amberlite IRN-78 anion-exchange resin (Alfa). The resulting solution was concentrated by rotary evaporation at 80 °C, and the final hydroxide concentration was determined by titration using 0.1 M HCl and phenolphthalein as an indicator. 1,2,3-Trimethylimidazolium (123TMI) hydroxide and 1,2,3,4-Tetramethylimidazolium (1234TMI) hydroxide, which are selective for the formation of PST-21 (PWO) and PST-22 (PWW) or RUB-13 (RTH), respectively, depending on the gel Si/Al and HF/OSDA ratios, were synthesized following the procedures described in our previous work.[S1]

S1.2. Zeolite Synthesis

In a typical aluminosilicate preparation, 1.0 mmol $Al(OH)_3$ and 10.0 mmol OSDA hydroxide were mixed in a Nalgene bottle for 1 hour. To the resulting solution, 20 mmol TEOS was added and the mixture subsequently stirred for 2 hours. The resulting mixture was then heated at 80 ^{o}C to remove liberated ethanol and excess H_2O. Finally, hydrofluoric acid was added to give a composition of $0.50R{\cdot}x HF{\cdot}0.1Al_2O_3{\cdot}1.0SiO_2{\cdot}5.0H_2O$, where R is one of the OSDAs prepared here and x is varied between $0.5 < x < 1.5$, and the mixture stirred by hand. The final synthesis mixture was then transferred into a 23-mL Teflon-lined autoclave and heated under rotation (60 rpm) at 160 °C for 14-21 days.

S1.2. Characterization

Powder X-ray diffraction (PXRD) data were recorded on a PANalytical X´Pert diffractometer (Cu Kα radiation, λ =1.54186 Å) with an X´Celerator detector. Elemental analysis for Si and Al was performed using a Shimadzu ICPE-9000 inductively coupled plasma spectrometer.

Thermogravimetric analyses (TGA) were carried out in air on an SII EXSTAR 6000 thermal analyzer, where the weight losses related to the combustion of OSDAs were confirmed by differential analyses (DTA) using the same analyzer. Crystal morphology and average size were determined using a JEOL JSM-6510 scanning electron microscope. N_2 sorption measurement were carried out at -196 °C on a Mirae SI nanoPorosity-XG analyzer.

Synchrotron PXRD data for as-synthesized 134TMP-PWO and 135TMP-PWW were collected on the 2D and 5A beamlines equipped with a ceramic furnace at the Pohang Accelerator Laboratory (PAL; Pohang, Korea) using monochromated X-rays (λ = 0.7000 and 0.6926 Å, respectively). Le Bail and Rietveld analyses were carried out using the GSAS suite of programs and EXPGUI graphical interface.[S2-S5] The refinement on the occluded OSDAs was performed using the rigid-body method.[S6] A summary of experimental and crystallographic data for 134TMP-PWO and 135TMP-PWW are shown in Table S1, and their atomic coordinates, thermal parameters, and selected bond lengths and angles are given in Tables S2-S5.

^{1}H and ^{13}C liquid nuclear magnetic resonance (NMR) measurements on OSDAs prepared here were performed in 5 mm quartz tubes using a Bruker AVANCE III 300 spectrometer. ^{1}H NMR spectra were measured at a ^{1}H frequency of 300.13 MHz with a π/2 rad pulse length of 11 ms and a recycle delay of 2 s. ^{13}C NMR spectra were recorded at a ^{13}C frequency of 75.475 MHz with a π/2 rad pulse length of 10.2 ms and a recycle delay of 1.5 s. Solid-state multinuclear magic angle spinning (MAS) NMR measurements were carried out using a Bruker AVANCE III 500 spectrometer. ^{27}Al and ^{29}Si MAS spectra at a spinning speed of 21.0 kHz were recorded at ^{27}Al and ^{29}Si frequencies of 130.351 and 99.357 MHz, π/6 and π/2 rad pulse lengths of 1.0 and 4.0 μs, recycle delays of 2.0 and 20 s, and acquisitions of ca. 100 and 500 pulse transients, respectively. The ^{27}Al chemical shifts are reported relative to an $Al(H_2O)_6^{3+}$ solution and TMS, respectively. ^{1}H-^{13}C cross polarization (CP) MAS NMR spectra at a spinning speed of 5.0 kHz were measured at a ^{13}C frequency of 125.795 MHz with a π/2 rad pulse length of 4.8 μs, a recycle delay of 3.0 s, and an acquisition of about 2000 pulse transients. ^{1}H MAS NMR spectra at a spinning speed of 10.0 kHz were collected a ^{1}H frequency of 500.57 MHz, π/2 rad pulse length of 4.2 μs, a recycle delay of 4.0 s, and an acquisition of about 32 pulse transients. The ^{29}Si, ^{13}C, and ^{1}H chemical shift is reported relative to TMS. ^{19}F MAS NMR spectra at spinning speeds of 10.0 and 15.0 kHz were

recorded at a ^{19}F frequency of 470.527 MHz, π/4 rad pulse length of 4.0 μs, a recycle delay of 5.0 s, and an acquisition of about 6000 pulse transients. The ^{19}F chemical shifts are referenced relative to $CFCl_3$.

S2. Computational Models and Methods

S2.1. Models: Unit cells considered

The zeolite phases obtained from experimental synthesis were considered from the molecular simulations point of view to calculate and compare their synthesis energies (E_{syn}) under different synthesis conditions. The zeolite phases used in the molecular simulations were: FER, ITE, ITW, PWO, PWW, and RTH. Since the '*c*' direction of the FER unit cell is too small for some of the OSDAs to rotate freely (c = 7.541 Å), we doubled the unit cell of FER when 124TMP, 125TMP and 134TMP are present to ensure that the Monte Carlo (zeoTsda) simulations run without interruption. The zeolite micropores were filled with OSDA molecules in such a manner that no more OSDA molecules could fit into the micropores without straining the structure. Unit cell representations of all pure-silica zeolites considered in this work are given, as an example, with 126TMP (Fig. S9).

The final composition of the unit cell models can be formulized as: $[OSDA]_a[Si_bAl_cO_{2(b+c)}(OH)_dF_e]$, where $a = c + d + e$. For pure-silica calculations (Table S6), since there are no framework Al atoms, or defects in the structure, the composition of the model becomes $[OSDA]_a[Si_bO_{2b}F_a]$. By contrast, for aluminosilicate calculations without F^- ions or defects (Table S7), the composition changes to $[OSDA]_a[Si_bAl_aO_{2(a+b)}]$. When defects are incorporated to the aluminosilicate structure (Table S8), the composition becomes $[OSDA]_a[Si_bAl_cO_{2(b+c)}(OH)_{(a-c)}]$.

S2.2. Calculations for pure-silica zeolites

The zeoTsda software[S7] was employed to find the optimal loading and position of OSDA molecules and fluoride anions, if fluoride is present inside zeolite cavities. The General

Utility Lattice Program (GULP)[S8] was used to perform a combination of Monte Carlo simulations with Lattice energy minimizations and find the best location for OSDAs at the optimal loading. The total energies of these optimized structures were then calculated through a single point energy calculation. Using the obtained total energies, the E_{syn}'s of pure-silica zeolites (Table S6) were calculated as explained in subsection S2.4.

S2.3. Calculations for aluminosilicate zeolites (with/without fluorides and defects)

For aluminosilicate zeolites, two other species (i.e., fluoride anions and framework defects) beside framework Al atoms were considered in order to balance the positive charge of the OSDAs. Of course, only those combinations that may aid in the interpretation of the experimental results were considered.

The Al incorporation into the zeolite framework was considered as follows: the unit cells, from the above calculations, for pure-silica zeolites fully packed with OSDA molecules were taken as a starting point. Then, the Si/Al ratio of structures was set either to: i) to compensate for all the positive charges of OSDAs (Table S7) or ii) to represent the Si/Al ratio of experimentally synthesized zeolites 123TMP-RTH and 135TMP-PWW (Si/Al～14; see Table S8). In the first set of simulations, the Al content in each unit cell was set by the user within the zeoTAl software, which generated 20 random Al distributions for each zeolite-OSDA pair following the Lowenstein's rule.[S9] These distributions were then optimized, and the E_{syn} values of the final geometries were calculated (Table S7).

In the second case, the software was expanded in order to be able to compensate for the positive charges of OSDAs not only by framework Al atoms but also by siloxy/silanol ($SiO^-\cdots HOSi$) defects. Using only a file containing the final geometry of the pure-silica zeolite with the packed OSDA molecules, the software automatically read the positive charges of the OSDA molecules and considered all combinations of Al + $SiO^-\cdots HOSi$ defects to counterbalance them. This also worked for files containing fluoride anions so that the remaining negative charges were generated from combinations of Al + $SiO^-\cdots HOSi$ defects.

In the initial simulations, we modelled the 1SiOH 1SiO^- cluster model across all structures, as

this defect is the simplest model. The 1SiOH 1SiO^- cluster model (i.e., a 1:1 connectivity defect) was generated from a random Si-O-Si linkage that was transformed into the SiO^-···HOSi pair, a hydrogen-bonded internal SiOH group with a net -1 charge. The atomic charge distribution is explained in the force field subsection S2.5. However, given the availability of ^{1}H DQ-SQ MAS NMR data for 123TMP-RTH, 134TMP-PWO, and 135TMP-PWW (see main text Fig. 3), which corresponds to different defect models (two hydrogen-bonded SiOH groups for PWO and PWW, and 1:1 connectivity defects for the RTH structure), we expanded the simulations to include multiple defect types. Specifically, we modelled the 1SiOH 1SiO^- and 3SiOH 1SiO^- cluster models for the corresponding zeolite-OSDA pairs.

The 3SiOH 1SiO^- cluster model, however, was developed using two distinct approaches: as a connectivity defect and as a vacancy defect. The 3SiOH 1SiO^- connectivity defect (2:1 connectivity defect) was generated following the model suggested by Brunklaus et al.[S10], where only two of the three SiOH groups in the defect site are close enough to the SiO^- group to form hydrogen bonds. The 3SiOH 1SiO^- vacancy defects(3:1 vacancy defect) was generated by removing a Si atom from one of the T-sites in the structure, thus creating a silanol nest with three SiOH groups interacting with a SiO^- group. These new defect models were subsequently optimized using periodic density functional theory (DFT) calculations performed with the CASTEP code,[S11] employing a similar methodology to that in our previous work.[S12] The goal of the DFT calculations was to accurately represent the geometries of the defect structures for 123TMP-RTH, 134TMP-PWO, and 135TMP-PWW, with a particular focus on accurately determining the O···O distances within the defect sites.

The O···O distances between SiO- and SiOH groups in the defects considered in Tables S9-S12 are given in Table S13. Additionally, the O···O distances for various defect types optimized via DFT calculations are provided in Table S14. An example of each structural defect type in the PWW framework is given in Figs. S10-S12.

S2.4. E_{syn} calculations

We employed the E_{syn} approach, similar to our previous studies,[S12,S13] which allowed us to compare the stabilities of zeolites according to a new parameter called E_{syn} that holds

similarities to the enthalpy of reaction. This could be exemplified by the following two synthesis eqns. from which two different zeolites are synthesized from the same reactants:

$$p_1\cdot\mathrm{OSDAOH} + m_1\cdot\mathrm{Si(OH)_4} + p_1\cdot\mathrm{Al(OH)_3} \rightarrow \mathrm{zeo_1\text{-}OSDA}(m_1,p_1) + w_1\cdot\mathrm{H_2O} \quad (1)$$

$$p_1\cdot\mathrm{OSDAOH} + m_1\cdot\mathrm{Si(OH)_4} + p_1\cdot\mathrm{Al(OH)_3} \rightarrow \mathrm{zeo_2\text{-}OSDA}(m_1,p_1) + w_2\cdot\mathrm{H_2O} + m_3\cdot\mathrm{Si(OH)_4} + p_3\cdot\mathrm{Al(OH)_3} \quad (2)$$

One zeolite ($\mathrm{zeo_1}$) with a Si/Al ratio of m_1/p_1 was obtained with water as a product, whereas the other zeolite ($\mathrm{zeo_2}$) with a Si/Al ratio of m_2/p_2 was synthesized with a different amount of water plus an excess of Si and Al monomers (m_3 and p_3, respectively). This can allow the energetic stability of the products to be directly compared, since both reactions have the same reactants.

If we assume that the synthesis is done under fluoride media, a small amount of F^- ions, call it q ($q < p$), will be incorporated into the structure. To have an overall net zero charge balance in the structure, we need to keep the negative charges equal to the number of OSDA molecules, 'p', thus, the number of 'OH^-' becomes '$p - q$'. Now, the number of $\mathrm{Si(OH)_4}$ and $\mathrm{Al(OH)_3}$ are equal to '$m + q$' and '$p - q$', respectively. Hence, we can write:

$$p\cdot\mathrm{OSDA} + q\cdot\mathrm{F^-} + (p-q)\cdot\mathrm{OH^-} + (m+q)\cdot\mathrm{Si}(OH)_4 + (p-q)\cdot\mathrm{Al}(OH)_3 \rightarrow [\mathrm{zeo}(m+q,p-q)\text{-}q\cdot\mathrm{F^-} - p\mathrm{OSDA}] + 2\cdot(m+p)\cdot\mathrm{H_2O} \quad (3)$$

When the SiOH $1SiO^-$ defect (1:1 connectivity defect) is formed in the framework ($\mathrm{SiOSi} + \mathrm{OH^-} \rightarrow \mathrm{SiOH} + \mathrm{SiO^-}$), we can describe them using the following synthesis eqn.:

$$[\mathrm{zeo}]^{-p} + d\cdot\mathrm{OH^-} \rightarrow [\mathrm{zeo}(m,p,d)]^{-(p+d)} \quad (4a)$$

where 'd' is the number of 1:1 connectivity defects ($\mathrm{SiO^-\cdots HOSi}$) formed in the framework, which does not change the total number of T-atoms. If we combine eqn. 3 and 4a considering a net zero charge balance in the structure, we get:

$$(p+d)\cdot\mathrm{OSDA} + q\cdot\mathrm{F^-} + (p-q+d)\cdot\mathrm{OH^-} + (m+q)\cdot\mathrm{Si(OH)_4} + (p-q)\cdot\mathrm{Al(OH)_3} \rightarrow$$

$$[\mathrm{zeo}(m+q,p-q)\text{-}q\cdot\mathrm{F}^{-}\text{-}d\text{-}(p+d)\cdot\mathrm{OSDA}]+2\cdot(m+p)\cdot\mathrm{H_2O} \quad (5a)$$

The corresponding reaction energy per T-atom ($m + p$), i.e., E_{syn}, is as follows:

$$E_{\mathrm{syn}} = E_{\text{zeolite-OSDAF}} + 2\cdot E_{\mathrm{H_2O}} - \frac{(p-q)+d}{m+p}\cdot E_{\mathrm{OSDAOH}} - \frac{(p-q)}{(m+p)}\cdot E_{\mathrm{Al(OH)_3}} - \frac{q}{m+p}\cdot E_{\mathrm{OSDAF}} - \frac{m+q}{m+p}\cdot E_{\mathrm{Si(OH)_4}} \quad (6a)$$

where E_{syn} is the synthesis energy of the reaction, $E_{\text{zeolite-OSDAF}}$ the energy of a zeolite-OSDAF pair with a given Si/Al ratio, E_{OSDAOH} and E_{OSDAF} the energies of the OSDA neutralized with hydroxide and fluoride anions, respectively, '*d*' is the number of defects in the framework, '*p* + *d*' and '*q*' the numbers of OSDA molecules and fluoride anions, respectively. The number of Al atoms is '*p* - *q*', and '*m* + *q*' is the number of Si, leading to a total number of tetrahedral atoms (T-atoms) of (*m* + *q*) + (*p* - *q*) = *m* + *p*. Also, since the total cationic OSDA charge is '*p* + *d*', and the negative charge is counterbalanced by Al(*p* - *q*), fluoride(*q*), and defects (*d*), giving a total of (*p* - *q*) + *q* + *d* = *p* + *d*, then the electroneutrality condition is followed. Since the energies of H_2O, $Si(OH)_4$, and $Al(OH)_3$ are fixed, the E_{syn} calculation is not more complex than the usual calculation of the total energy of the system (i.e., zeolite + OSDA).

When the 3SiOH 1SiO$^-$ defect model (2:1 connectivity or 3:1 vacancy defect) is formed in the framework ($2\mathrm{SiOSi} + \mathrm{OH^-} + \mathrm{H_2O} \rightarrow 3\mathrm{SiOH} + \mathrm{SiO^-}$, we can describe them using the following synthesis eqn.:

$$[\mathrm{zeo}]^{-p} + d\cdot\mathrm{H_2O} + d\cdot\mathrm{OH^-} \rightarrow [\mathrm{zeo}(m,p,d)]^{-(p+d)} \quad (4b)$$

where '*d*' is the number of 2:1 connectivity or 3:1 vacancy defects (3SiOH + SiO$^-$) formed in the framework, which in the latter applies with a correspondingly lower number of '*d*' missing Si atoms, that will be still described as '*m*'. If we combine eqn. 3 and 4b, considering a net zero charge balance in the structure, we get:

$$(p+d)\cdot\mathrm{OSDA} + q\cdot\mathrm{F^-} + (p-q+d)\cdot\mathrm{OH^-} + (m+q)\cdot\mathrm{Si(OH)_4} +$$
$$(p-q)\cdot\mathrm{Al(OH)_3} + d\cdot\mathrm{H_2O} \rightarrow \mathrm{zeo}(m+q,p-q)\text{-}q\cdot\mathrm{F^-}\text{-}d[\text{-}(p+d)\cdot\mathrm{OSDA}]+2\cdot(m+p)\cdot\mathrm{H_2O} \quad (5b)$$

The corresponding reaction energy per T-atom ($m + p$), i.e., E_{syn}, is as follows:

$$E_{\text{syn}} = E_{\text{zeolite-OSDAF}} + \frac{2(m+p) - d}{m+p} \cdot E_{\text{H}_2\text{O}} - \frac{(p - q) + d}{m+p} \cdot E_{\text{OSDAOH}} - \frac{(p - q)}{(m+p)} \cdot E_{\text{Al(OH)}_3} - \frac{q}{m+p} \cdot E_{\text{OSDAF}} - \frac{m+q}{m+p} \cdot E_{\text{Si(OH)}_4} \quad (6b)$$

The zeolite-OSDAF model includes the $SiO^{-}\cdots HOSi$ defects in the structure and has to be calculated with the new force field parameters presented in section S2.5. This allows a prediction of the product obtained using a specific OSDA, when considering all experimentally obtained competing phases in pure-silica or aluminosilicate gels, with the most stable being that with lowest E_{syn} value.

S2.5. Force field used

In this study, we used a modified version of a force field presented in our previous work[S14] in order to describe the aluminosilicate structures with $SiO^{-}\cdots HOSi$ defects. A Lennard-Jones potential (LJ, eqn. 8) was used to define the van der Waals interactions, while the electrostatic interactions were described by the Coulomb potential (eqn. 7). The parameters of these potentials are given in Tables S15 and S16.

$$U^{\text{Coulomb}}(\text{r}_{\text{ij}}) = q_{\text{i}} q_{\text{j}} / 4\pi\epsilon_0 r_{\text{ij}} \quad (7)$$

$$U^{\text{LJ}}(\text{r}_{\text{ij}}) = (\text{A}/r_{\text{ij}}^{12}) - (\text{B}/r_{\text{ij}}^{6}) \quad (8)$$

Three-body potentials (eqn. 9) were utilized to describe the bonded interactions, with the corresponding parameters given in Table S17. The bond between the silanol oxygen and the hydrogen was modelled by a Morse potential (eqn. 10) with the parameters given in Table S18.

$$U^{\text{three-body}}(\Theta_{\text{ijk}}) = k_{\Theta}(\Theta_{\text{ijk}} - \Theta_0)^2 \quad (9)$$

$$U^{\text{morse}}(\text{r}_{\text{ij}}) = E_0 \left[\{1 - \exp[-k(r_{\text{ij}} - r_0)]\}^2 - 1\right] \quad (10)$$

Finally, since a bond breakage between some O and H atoms of surface silanol groups caused

by strong electrostatic interactions of H with neighboring O atoms was observed, a repulsive Buckingham potential (eqn. 11) between H and O atoms that are not directly bonded to each other was included. The parameters for this potential are given in Table S19.

$$U^{\text{buck}}(r_{\text{ij}}) = A\exp\left(-\frac{r_{\text{ij}}}{\rho}\right) - \left(\frac{C}{r_{\text{ij}}^{6}}\right) \tag{11}$$

Although other parameterized atoms have not been used in this study, they are available from our previous study[S14] and are also included (Table S20) to facilitate a full access to this general force field.

The charges of Si and O atoms for the central SiO_4 tetrahedral in Si-(O_4)-($SiO_{3/2}$)$_4$ units are 2.1 and -1.05, respectively, corresponding to an overall zero charge, while those of Al and O atoms for the central AlO_4^- tetrahedral in Al-(O_4)-($SiO_{3/2}$)$_4$ units are 1.575 and -1.16875, respectively, giving an overall -1 charge (1.575 - 1.16875 × 4 + 2.1 × 4 - 1.05 × 6). This enables the AlO_4^- tetrahedral to balance the positive charge of OSDA in the unit cell. Similarly, the charges of $SiO^-\cdots HOSi$ defects (Si31-O31$^-\cdots$H2-O32-Si32) lead to an overall -1 charge (1.8 - 1.225 - 1.05 × 6/2 + 0.375 – 0.9 + 2.1). Hence, the defects can also be incorporated for charge balancing instead of, or additionally to, the AlO_4^- tetrahedral unit.

Table S1 Crystallographic and experimental parameters for the Rietveld Refinement of the Synchrotron PXRD Data of as-synthesized 134TMP-PWO and 135TMP-PWW

	134TMP-PWO	135TMP-PWW
refined unit cell formula	$\|(134TMP)_2\|[Si_{20}O_{40}]$	$\|(135TMP)_4\|[Si_{40}O_{80}]$
crystal system	monoclinic	monoclinic
space group	$P2_1/c$ (no. 14)	$C2/c$ (no. 15)
a (Å)	9.3494(15)	20.8038(6)
b (Å)	11.9607(34)	11.76087(35)
c (Å)	11.0756(31)	10.96997(34)
β (°)	93.013(22)	118.7445(16)
unit cell volume (Å^3)	1236.8(5)	2353.29(15)
X-ray source	2D beamline, PAL	5A beamline, PAL
wavelength (Å)	0.7000	0.6926
2θ range (°)	3-41	3-50
step size (°)	0.025	0.0075
no. of data points	1521	6267
no. of restraints	50	50
no. of parameters	81	81
R_{ap} (%)	3.52	8.84
R_{up} (%)	4.51	12.38
R_{eap} (%)	1.62	2.85
R_F^2 (%)	6.588	11.601
GOF	3.60	4.52
$(\Delta/\sigma)_{max}$	0.02	0.02
$(\Delta/\sigma)_{mean}$	0.00	0.00

Table S2 Atomic coordinates and thermal parameters for as-synthesized 134TMP-PWO

Atom	*x*	*y*	*z*	Occupancy	T_{isa}	Multiplicity
Si1	0.1587(8)	0.4044(7)	0.2222(7)	1	0.01	4
Si2	0.0865(8)	0.8273(6)	0.4677(7)	1	0.01	4
Si3	0.1436(8)	0.1646(7)	0.3260(7)	1	0.01	4
Si4	0.3259(8)	0.4888(7)	0.0016(8)	1	0.01	4
Si5	0.0462(9)	0.5772(6)	0.3904(7)	1	0.01	4
O1	0.1533(7)	0.5092(5)	0.3100(6)	1	0.01	4
O2	0.0084(6)	0.3834(7)	0.1438(5)	1	0.01	4
O3	0.1943(9)	0.2912(4)	0.2991(7)	1	0.01	4
O4	0.2835(7)	0.4275(7)	0.1266(5)	1	0.01	4
O5	0.7629(6)	0.3953(5)	0.0107(9)	1	0.01	4
O6	0.0066(6)	0.1650(8)	0.4123(5)	1	0.01	4
O7	0.1134(9)	0.6960(4)	0.4378(8)	1	0.01	4
O8	0.2717(7)	0.0937(5)	0.3911(6)	1	0.01	4
O9	0.0940(7)	0.1071(7)	0.1981(5)	1	0.01	4
O10	0.5	0	0.5	1	0.01	2
O11	0	0	0	1	0.01	2
N1	0.573(6)	0.389(5)	0.402(5)	0.5	0.01	4
C2	0.569(6)	0.501(5)	0.375(5)	0.5	0.01	4
C3	0.513(6)	0.579(5)	0.455(5)	0.5	0.01	4
C4	0.460(6)	0.540(5)	0.564(5)	0.5	0.01	4
C5	0.464(6)	0.425(6)	0.589(5)	0.5	0.01	4
C6	0.521(6)	0.351(5)	0.507(6)	0.5	0.01	4
Cm1	0.633(7)	0.312(6)	0.316(7)	0.5	0.01	4
Cm3	0.513(7)	0.701(5)	0.421(7)	0.5	0.01	4
Cm4	0.398(7)	0.617(7)	0.656(6)	0.5	0.01	4

Table S3 Atomic coordinates and thermal parameters for as-synthesized 135TMP-PWW

Atom	*x*	*y*	*z*	Occupancy	K_{iso}	Multiplicity
Si1	0.83736(25)	0.6502(4)	0.3671(5)	1	0.0165(11)	8
Si2	0.71109(24)	0.5742(4)	0.4301(5)	1	0.0165(11)	8
Si3	0.82820(25)	0.5861(4)	0.7522(5)	1	0.0165(11)	8
Si4	0.91607(21)	0.7452(4)	0.6640(5)	1	0.0165(11)	8
Si5	0.72807(27)	0.32630(35)	0.3651(4)	1	0.0165(11)	8
O1	0.76081(29)	0.6284(6)	0.3668(7)	1	0.0138(17)	8
O2	0.85932(31)	0.5391(4)	0.3104(7)	1	0.0138(17)	8
O3	0.90108(30)	0.6784(5)	0.5228(4)	1	0.0138(17)	8
O4	0.82969(32)	0.7577(4)	0.2697(4)	1	0.0138(17)	8
O5	0.75991(31)	0.5766(6)	0.5974(4)	1	0.0138(17)	8
O6	0.63705(25)	0.6446(4)	0.3800(6)	1	0.0138(17)	8
O7	0.69156(31)	0.44397(29)	0.3779(6)	1	0.0138(17)	8
O8	0.89294(29)	0.6610(5)	0.7533(6)	1	0.0138(17)	8
O9	0.80020(31)	0.6448(6)	0.8516(6)	1	0.0138(17)	8
O10	0.5	0.2793(7)	0.75	1	0.0138(17)	4
O11	0.75	0.25	0.5	1	0.0138(17)	4
N1	0.5002(7)	0.1853(7)	0.2735(7)	0.5	0.023(5)	8
C2	0.5308(8)	0.2510(7)	0.3889(7)	0.5	0.023(5)	8
C3	0.5277(7)	0.3689(7)	0.3798(7)	0.5	0.023(5)	8
C4	0.4913(7)	0.4168(7)	0.2465(7)	0.5	0.023(5)	8
C5	0.4591(7)	0.3489(7)	0.1269(7)	0.5	0.023(5)	8
C6	0.4649(7)	0.2314(7)	0.1450(7)	0.5	0.023(5)	8
C1m	0.5068(8)	0.0608(7)	0.2914(7)	0.5	0.023(5)	8
C3m	0.5635(9)	0.4378(7)	0.5109(7)	0.5	0.023(5)	8
C5m	0.4195(10)	0.3972(7)	-0.0172(7)	0.5	0.023(5)	8

Table S4 Selected bond lengths and angles for as-synthesized 134TMP-PWO

Bond length (Å)		Bond angle (°)	
Si1-O1	1.589(10)	O1-Si1-O2	113.1(6)
Si1-O2	1.632(10)	O1-Si1-O3	110.4(6)
Si1-O3	1.624(10)	O1-Si1-O4	108.0(6)
Si1-O4	1.639(10)	O2-Si1-O3	107.3(6)
Si2-O2	1.627(10)	O2-Si1-O4	107.7(5)
Si2-O5	1.633(9)	O3-Si1-O4	110.2(6)
Si2-O6	1.629(10)	O2-Si2-O5	109.7(6)
Si2-O7	1.627(9)	O2-Si2-O6	107.7(5)
Si3-O3	1.620(10)	O2-Si2-O7	109.1(6)
Si3-O6	1.637(10)	O5-Si2-O6	110.2(6)
Si3-O8	1.607(10)	O5-Si2-O7	111.6(6)
Si3-O9	1.621(10)	O6-Si2-O7	108.4(6)
Si4-O4	1.634(10)	O3-Si3-O6	110.5(6)
Si4-O5	1.617(10)	O3-Si3-O8	111.0(6)
Si4-O8	1.632(10)	O3-Si3-O9	108.0(6)
Si4-O10	1.635(7)	O6-Si3-O8	109.1(6)
Si5-O1	1.597(10)	O6-Si3-O9	108.3(5)
Si5-O7	1.630(9)	O8-Si3-O9	109.9(6)
Si5-O9	1.634(10)	O4-Si4-O5	108.1(6)
Si5-O11	1.602(8)	O4-Si4-O8	106.5(6)
Si-O (avg.)	1.623	O4-Si4-O10	109.4(5)
N1-C2	1.3636(4)	O5-Si4-O8	108.5(6)
N1-C6	1.36352(33)	O5-Si4-O10	115.8(5)
N1-Cm1	1.46479(29)	O8-Si4-O10	108.1(5)
C2-C3	1.40385(27)	O1-Si5-O7	112.4(6)
C3-C4	1.41447(35)	O1-Si5-O9	106.5(5)
C3-Cm3	1.5045(4)	O1-Si5-O11	109.3(5)
C4-C5	1.4006(4)	O7-Si5-O9	106.6(6)
C4-Cm4	1.50905(30)	O7-Si5-O11	111.9(5)
C5-C6	1.39421(27)	O9-Si5-O11	109.9(5)
		O-Si-O (avg.)	109.44
		Si1-O1-Si5	141.6(6)
		Si1-O2-Si2	152.5(6)
		Si1-O3-Si3	145.3(7)
		Si1-O4-Si4	146.6(6)
		Si2-O5-Si4	150.9(5)
		Si2-O6-Si3	160.7(5)
		Si2-O7-Si5	147.8(7)
		Si3-O8-Si4	148.2(6)
		Si3-O9-Si5	143.2(6)
		Si4-O10-Si4	180
		Si5-O11-Si5	180
		C2-N1-C6	120.5375(35)
		C2-N1-Cm1	118.904(15)
		C6-N1-Cm1	120.559(18)
		N1-C2-C3	121.160(15)
		C2-C3-C4	118.785(18)
		C2-C3-Cm3	119.020(16)
		C4-C3-Cm3	122.1949(26)
		C3-C4-C5	118.794(4)
		C3-C4-Cm4	123.141(18)
		C5-C4-Cm4	118.064(15)
		C4-C5-C6	120.174(15)
		N1-C6-C5	120.547(18)

Table S5 Selected bond lengths and angles for as-synthesized 135TMP-PWW

Bond length (Å)		Bond angle (°)	
Si1-O1	1.611(4)	O1-Si1-O2	109.59(32)
Si1-O2	1.605(4)	O1-Si1-O3	110.05(33)
Si1-O3	1.615(4)	O1-Si1-O4	109.88(32)
Si1-O4	1.613(4)	O2-Si1-O3	109.61(32)
Si2-O1	1.628(4)	O2-Si1-O4	109.71(32)
Si2-O5	1.615(4)	O3-Si1-O4	107.98(32)
Si2-O6	1.596(4)	O1-Si2-O5	107.26(32)
Si2-O7	1.617(4)	O1-Si2-O6	110.87(34)
Si3-O2	1.612(4)	O1-Si2-O7	108.85(32)
Si3-O5	1.610(4)	O5-Si2-O6	110.95(33)
Si3-O8	1.604(4)	O5-Si2-O7	109.42(32)
Si3-O9	1.618(4)	O6-Si2-O7	109.44(32)
Si4-O3	1.627(4)	O2-Si3-O5	109.69(33)
Si4-O6	1.619(4)	O2-Si3-O8	108.84(32)
Si4-O8	1.620(4)	O2-Si3-O9	109.20(32)
Si4-O10	1.586(4)	O5-Si3-O8	110.98(33)
Si5-O4	1.604(4)	O5-Si3-O9	108.61(31)
Si5-O7	1.617(4)	O8-Si3-O9	109.50(33)
Si5-O9	1.613(4)	O3-Si4-O6	108.18(32)
Si5-O11	1.598(4)	O3-Si4-O8	107.71(32)
Si-O (avg.)	1.611	O3-Si4-O10	109.93(31)
N1-C2	1.352800(30)	O6-Si4-O8	108.08(32)
N1-C6	1.35162(4)	O6-Si4-O10	111.88(33)
N1-C1m	1.47502(4)	O8-Si4-O10	110.91(32)
C2-C3	1.38994(4)	O4-Si5-O7	109.61(31)
C3-C4	1.40167(4)	O4-Si5-O9	109.77(32)
C3-C3m	1.49979(4)	O4-Si5-O11	108.98(30)
C4-C5	1.40107(4)	O7-Si5-O9	108.92(31)
C5-C6	1.39326(4)	O7-Si5-O11	109.71(32)
C5-C5m	1.49952(5)	O9-Si5-O11	109.83(29)
		O-Si-O (avg.)	109.46
		Si1-O1-Si2	153.0(5)
		Si1-O2-Si3	139.7(4)
		Si1-O3-Si4	142.2(4)
		Si1-O4-Si5	142.8(4)
		Si2-O5-Si3	162.4(5)
		Si2-O6-Si4	157.7(4)
		Si2-O7-Si5	142.5(4)
		Si3-O8-Si4	145.4(4)
		Si3-O9-Si5	143.5(4)
		Si4-O10-Si4	150.7(6)
		Si5-O11-Si5	180
		C2-N1-C6	121.4938(22)
		N1-C2-C3	121.2087(14)
		C2-C3-C4	117.3312(8)
		C2-C3-C3m	119.0654(14)
		C4-C3-C3m	123.6019(22)
		C3-C4-C5	121.5478(22)
		C4-C5-C6	117.5604(15)
		C4-C5-C5m	122.9866(21)
		C6-C5-C5m	119.4525(6)
		N1-C6-C5	120.8532(7)

Table S6 Synthesis energies (E_{syn}'s) of pure-silica zeolites in fluoride media

OSDA[a]	Zeolite[b]	Energy per Si atom (eV)	No. of OSDAs per unit cell	No. of Si atoms per unit cell	E_{syn} per Si atom (eV)	Rank
123TMP	FER	-40.916	4	36	-0.269	3
	ITE	-40.832	6	64	-0.210	5
	ITW	-40.961	2	24	-0.354	1
	PWO	-40.846	2	20	-0.215	4
	PWW	-40.816	4	40	-0.185	6
	RTH	-40.935	4	32	-0.269	3
124TMP	FER	-40.876	8	72	-0.241	3
	ITE	-40.833	6	64	-0.198	6
	ITW	-40.986	2	24	-0.367	1
	PWO	-40.855	2	20	-0.210	4
	PWW	-40.854	4	40	-0.209	5
	RTH	-40.958	4	32	-0.275	2
125TMP	FER	-40.798	8	72	-0.250	3
	ITE	-40.944	8	64	-0.265	2
	ITW	-40.982	2	24	-0.365	1
	PWO	-40.818	2	20	-0.176	5
	PWW	-40.792	4	40	-0.150	6
	RTH	-40.909	4	32	-0.229	4
126TMP	FER	-40.887	4	36	-0.263	3
	ITE	-40.850	8	64	-0.209	4
	ITW	-40.914	2	24	-0.324	1
	PWO	-40.815	2	20	-0.205	6
	PWW	-40.818	4	40	-0.207	5
	RTH	-40.945	4	32	-0.304	2
134TMP	FER	-40.926	8	72	-0.242	3
	ITE	-40.981	8	64	-0.273	2
	ITW	-41.009	2	24	-0.373	1
	PWO	-40.884	2	20	-0.219	4
	PWW	-40.848	4	40	-0.183	5
	RTH	-40.762	2	32	-0.162	6
135TMP	FER	-40.829	4	36	-0.176	6
	ITE	-40.807	5	64	-0.176	6
	ITW	-40.958	2	24	-0.318	1
	PWO	-40.856	2	20	-0.185	4
	PWW	-40.897	4	40	-0.227	3
	RTH	-41.023	4	32	-0.308	2

[a] For each OSDA, the lowest synthesis energy is highlighted in yellow background.

[b] F^- ion locations within the small cages and larger cavities were: *fer* [5^4] for FER (left figure); *rth* [4^45^4] for ITE and RTH (central figure); [4^25^1] region of *t-pwo* and *t-pww* cavities within PWO (right figure) and PWW, respectively; and *d4r* [4^6] for ITW (not shown).

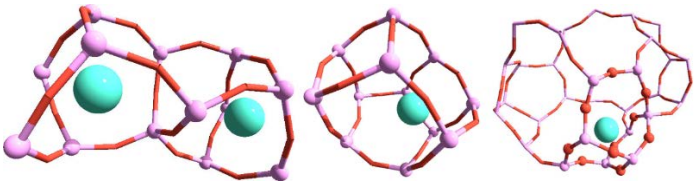

Table S7 E_{syn} values of aluminosilicate zeolites without fluoride anions and without SiO^-···HOSi defects[a]

OSDA	Zeolite	Energy per T-atom (eV)	No. of OSDAs per unit cell	No. of T-atoms per unit cell	Si/Al ratio	Avg. E_{syn} per T-atom[a] (eV)	Rank
123TMP	FER	-39.871	4	36	8	-0.914	3
	ITE	-39.757	8	64	7	-0.997	2
	ITW	-39.966	2	24	11	-0.633	6
	PWO	-39.959	2	20	9	-0.841	5
	PWW	-39.968	4	40	9	-0.849	4
	RTH	-39.802	4	32	7	-1.043	1
124TMP	FER	-39.862	8	72	8	-0.881	3
	ITE	-39.746	8	64	7	-0.967	2
	ITW	-40.098	2	24	11	-0.750	6
	PWO	-39.981	2	20	9	-0.838	5
	PWW	-40.003	4	40	9	-0.869	4
	RTH	-39.803	4	32	7	-1.030	1
125TMP	FER	-39.887	8	72	8	-0.923	3
	ITE	-39.747	8	64	7	-0.968	2
	ITW	-40.091	2	24	11	-0.766	6
	PWO	-39.956	2	20	9	-0.841	4
	PWW	-39.944	4	40	9	-0.820	5
	RTH	-39.783	4	32	7	-1.008	1
126TMP	FER	-39.846	4	36	8	-0.896	3
	ITE	-39.756	8	64	7	-1.020	1
	ITW	-40.082	2	24	11	-0.750	6
	PWO	-39.927	2	20	9	-0.835	4
	PWW	-39.922	4	40	9	-0.827	5
	RTH	-39.723	4	32	7	-0.982	2
134TMP	FER	-39.889	8	72	8	-0.899	3
	ITE	-39.828	8	64	7	-1.027	2
	ITW	-40.131	2	24	11	-0.758	6
	PWO	-39.985	2	20	9	-0.851	5
	PWW	-40.020	4	40	9	-0.869	4
	RTH	-39.845	4	32	7	-1.04	1
135TMP	FER	-39.921	4	36	8	-0.912	3
	ITE	-39.838	8	64	7	-1.002	2
	ITW	-40.148	2	24	11	-0.762	6
	PWO	-39.994	2	20	9	-0.849	4
	PWW	-39.955	4	40	9	-0.809	5
	RTH	-39.836	4	32	7	-1.019	1

[a] For each OSDA, the lowest synthesis energy is highlighted in yellow background.

Table S8 E_{syn} values of aluminosilicate (Si/Al ~ 14) zeolites with 1:1 connectivity defects but without fluoride ions[a]

OSDA	Zeolite	Energy per T-atom (eV)	No. of OSDAs per unit cell	No. of Al atoms per unit cell	No. of defects per unit cell	No. of T-atoms per unit cell	Si/Al ratio	Avg. E_{syn} per T-atom[a] (eV)	Rank
123TMP	FER	-40.251	4	2	2	36	17.0	-0.172	4
	ITE	-40.062	8	4	4	64	15.0	-0.035	6
	ITW	-40.247	2	1	1	24	23.0	-0.065	5
	PWO	-40.119	4	3	1	40	12.3	-0.503	2
	PWW	-40.122	4	3	1	40	12.3	-0.505	1
	RTH	-40.243	4	2	2	32	15.0	-0.215	3
135TMP	FER	-40.266	4	2	2	36	17.0	-0.145	5
	ITE	-40.209	8	4	4	64	15.0	-0.135	6
	ITW	-40.403	2	1	1	24	23.0	-0.189	4
	PWO	-40.153	4	3	1	40	12.3	-0.499	1
	PWW	-40.126	4	3	1	40	12.3	-0.472	2
	RTH	-40.284	4	2	2	32	15.0	-0.210	3

[a] For each OSDA, the lowest synthesis energy is highlighted in yellow background.

Table S9 E_{syn} values of aluminosilicate 123TMP-RTH zeolite with different chemical compositions, with Al atoms, fluoride ions, and/or defects present, compensating the positive charges of OSDAs

Anionic content	Energy per T-atom (eV)	No. of OSDAs per unit cell	No. of Al atoms per unit cell	No. of F^- ions per unit cell	No. of defects per unit cell	Si/Al ratio	Avg. E_{syn} per T-atom (eV)
4 Al	-39.811	4	4	0	0	7.0	-1.043
2 Al, 2 F^-	-40.344	4	2	2	0	15.0	-0.627
2 Al, 1 F^-, 1:1 connectivity defect	-40.268	4	2	1	1	15.0	-0.396
2 Al, 2 1:1 connectivity defects	-40.198	4	2	0	2	15.0	-0.215
2 Al, 2 2:1 connectivity defects	-40.851	4	2	0	2	15.0	-0.265
2 Al, 2 3:1 vacancy defects	-41.015	4	2	0	2	14.0	-0.422

Table S10 E_{syn} values of pure-silica 135TMP-ITW zeolite with different chemical compositions, with fluoride ions, and/or defects present, compensating the positive charges of OSDAs

Anionic content	Energy per T-atom (eV)	No. of OSDAs per unit cell	No. of F^- ions per unit cell	No. of defects per unit cell	Avg. E_{syn} per T-atom (eV)
2 F^-	-40.958	2	2	0	-0.318
1 F^-, 1:1 connectivity defect	-40.773	2	1	1	0.074
2 1:1 connectivity defects	-40.682	2	0	2	0.371

Table S11 E_{syn} values of aluminosilicate 134TMP-PWO zeolite with different chemical compositions, with Al atoms, fluoride ions, and/or defects present, compensating the positive charges of OSDAs

Anionic content	Energy per T-atom (eV)	No. of OSDAs per unit cell	No. of Al atoms per unit cell	No. of F^- ions per unit cell	No. of defects per unit cell	Si/Al ratio	Avg. E_{syn} per T-atom (eV)
2 Al	-39.985	2	2	0	0	9.0	-0.851
3 Al, 1 F^- (enlarged)[a]	-40.206	4	3	1	0	12.3	-0.682
3 Al, 1:1 connectivity defect (enlarged)	-40.145	4	3	0	1	12.3	-0.497
3 Al, 2:1 connectivity defect (enlarged)	-40.374	4	3	0	1	12.3	-0.509
3 Al, 3:1 vacancy defect (enlarged)	-40.439	4	3	0	1	12.0	-0.590

[a] The unit cell is doubled to 2 × 1 × 1.

Table S12 E_{syn} values of aluminosilicate 135TMP-PWW zeolite with different chemical compositions, with Al atoms, fluoride ions, and/or defects present, compensating the positive charges of OSDAs

Anionic content	Energy per T-atom (eV)	No. of OSDAs per unit cell	No. of Al atoms per unit cell	No. of F^- ions per unit cell	No. of defects per unit cell	Si/Al ratio	Avg. E_{syn} per T-atom (eV)
4 Al	-39.955	4	4	0	0	9.0	-0.809
3 Al, 1 F^-	-40.180	4	3	1	0	12.3	-0.651
3 Al, 1:1 connectivity defect	-40.126	4	3	0	1	12.3	-0.472
3 Al, 2:1 connectivity defect	-40.351	4	3	0	1	12.3	-0.481
3 Al, 3:1 vacancy defect	-40.430	4	3	0	1	12.0	-0.576

Table S13 O···O distances between SiO^- and SiOH groups for models of zeolites with 1:1 connectivity defects considered in Tables S9-S12 computed by force field calculations

Zeolite	Anion composition	O···O distance in defect 1	O···O distance in defect 2	Avg. O···O distance	Global average
123TMP-RTH (Table S9)	2 Al, 2 defects	2.501	2.423	2.462	2.450
	2 Al, 2 defects	2.427	2.419	2.423	
	2 Al, 2 defects	2.414	2.499	2.457	
	2 Al, 2 defects	2.462	2.421	2.441	
	2 Al, 2 defects	2.522	2.407	2.465	
123TMP-RTH (Table S9)	2 Al, 1 F^-, 1 defect	2.451		2.451	2.474
	2 Al, 1 F^-, 1 defect	2.628		2.628	
	2 Al, 1 F^-, 1 defect	2.478		2.478	
	2 Al, 1 F^-, 1 defect	2.404		2.404	
	2 Al, 1 F^-, 1 defect	2.411		2.411	
135TMP-ITW (Table S10)	2 defects	2.407	2.501	2.454	2.459
	2 defects	2.428	2.513	2.470	
	2 defects	2.481	2.516	2.499	
	2 defects	2.416	2.437	2.426	
	2 defects	2.431	2.457	2.444	
135TMP-ITW (Table S10)	1 F^-, 1 defect	2.468		2.468	2.446
	1 F^-, 1 defect	2.467		2.467	
	1 F^-, 1 defect	2.432		2.432	
	1 F^-, 1 defect	2.431		2.431	
	1 F^-, 1 defect	2.432		2.432	
134TMP-PWO (Table S11)	3 Al, 1 defect	2.473		2.473	2.549
	3 Al, 1 defect	2.472		2.472	
	3 Al, 1 defect	2.886		2.886	
	3 Al, 1 defect	2.452		2.452	
	3 Al, 1 defect	2.460		2.460	
135TMP-PWW (Table S12)	3 Al, 1 defect	2.431		2.431	2.442
	3 Al, 1 defect	2.461		2.461	
	3 Al, 1 defect	2.439		2.439	
	3 Al, 1 defect	2.447		2.447	
	3 Al, 1 defect	2.433		2.433	

Table S14 O···O distances between SiO^- and SiOH groups for various defect models of 123TMP-RTH, 134TMP-PWO and 135TMP-PWW computed by DFT calculations. The defect models were chosen from the work of Brunklaus et al.[S10] Numbers in parenthesis correspond to the average O···O distances computed by force field calculations

Zeolite	Defect type	O···O distance in defect 1	O···O distance in defect 2	Avg. O···O distance	Global average
123TMP-RTH	1:1 connectivity defect	2.40	2.48	2.44	2.44 (2.45)
		2.41	2.47	2.44	
		2.40	2.48	2.44	
		2.43	2.42	2.42	
		2.40	2.49	2.44	
123TMP-RTH	2:1 connectivity defect	2.47	2.47	2.47	2.48
		2.44	2.47	2.46	
		2.48	2.47	2.47	
		2.45	2.50	2.47	
		2.53	2.49	2.51	
123TMP-RTH	3:1 vacancy defect	2.50	2.58	2.54	2.56
		2.57	2.62	2.60	
		2.51	2.52	2.52	
		2.58	2.68	2.63	
		2.53	2.50	2.52	
134TMP-PWO	1:1 connectivity defect	2.42		2.42	2.43 (2.54)
		2.44		2.44	
		2.44		2.44	
		2.40		2.40	
		2.46		2.46	
134TMP-PWO	2:1 connectivity defect	2.44		2.44	2.46
		2.45		2.45	
		2.50		2.50	
		2.56		2.56	
		2.40		2.40	
134TMP-PWO	3:1 vacancy defect	2.51		2.51	2.56
		2.57		2.57	
		2.55		2.55	
		2.56		2.56	
		2.58		2.58	
134TMP-PWW	1:1 connectivity defect	2.43		2.43	2.43 (2.44)
		2.43		2.43	
		2.41		2.41	
		2.43		2.43	
		2.44		2.44	
135TMP-PWW	2:1 connectivity defect	2.52		2.52	2.52
		2.56		2.56	
		2.51		2.51	
		2.54		2.54	
		2.44		2.44	
135TMP-PWW	3:1 vacancy defect	2.53		2.53	2.58
		2.51		2.51	
		2.64		2.64	
		2.62		2.62	
		2.59		2.59	

Table S15 Species described in the force field with their corresponding atom types and electrostatic charges

Species	Atom type	Charge (e^-)	Ref.
framework Si	Si	2.100	S14
framework Si O	O2	-1.050	S14
framework Al	Al	1.575	S14
framework Al O	O1	-1.16875	S14
silanol (Si32-O32-H2)	Si32	2.100	S14
	O32	-0.900	S14
	H2	0.375	S14
siloxy (Si31-$O31^-$)	Si31	1.800	this work
	O31	-1.225	this work

Table S16 Lennard-Jones potential parameters of the species described in the force field[S14,a]

Pair	A (eV Å^{-12})	B (eV Å^{-6})
Si···Si	0.5601	0.0004
Si···Al	1.0153	0.0005
Al···Al	1.8405	0.0006
Si···O1	218.1689	0.9583
Si···O2	172.6992	0.1086
Si···O31	124.1989	0.1044
Si···O32	124.1989	0.1044
Al···O1	259.9127	0.0786
Al···O2	342.4165	0.0786
Al···O31	236.009	0.1309
Al···O32	236.009	0.1309
O1···O1	26877.9664	29.8306
O1···O2	26877.9664	29.8306
O1···O31	27097.4251	28.4516
O1···O32	27097.4251	28.4516
O2···O2	26877.9664	29.8306
O2···O31	27097.4251	28.4516
O2···O32	27097.4251	28.4516
O31···O31	27290.9346	27.1226
O31···O32	27290.9346	27.1226
O32···O32	27290.9346	27.1226

[a] Si and Al are generic framework Si and Al, respectively, and labels for $SiO^-\cdots HOSi$ defects are the same as those in Table S15.

Table S17 Three-body potential parameters of the species described in the force field (See eqn. 9)[S14,a]

Three-body	k_ϑ (eV rad^{-2})	Θ_0 (°)
O*x*–Si –O*x*	1.4944	109.470
O1–Al–O1	0.4747	109.470
Si–O2–Si	3.1731	142.712
Al–O1–Si	1.7875	140.831
O31–Si31–O*x*	1.4944	109.470
O32–Si32–O*x*	1.4944	109.470
Si32–O32–H2	1.3000	100.000

[a] Si and Al are generic framework Si and Al, respectively, and O*x* is any oxygen with x = 1 and 2. Labels for $SiO^-\cdots HOSi$ defects are the same as those in Table S15.

Table S18 Morse potential (O32-H2) parameters of the species described in the force field[S14,a]

Parameter	Value	Unit
E_0	7.0525	eV
k	2.1986	$Å^{-1}$
r_0	0.9476	Å

[a] See eqn. 10.

Table S19 Buckingham potential (O*x*···H*y*) parameters of the species described in the force field (See eqn. 11)[S15,*a*]

Parameter	Value	Unit
A	311.97	eV
ρ	0.25	Å
C	0.0	eV Å^{-6}

[*a*] O*x* is any oxygen with *x* = 1 and 2, and H*y* is any hydrogen with *y* = 2 and 3.

Table S20 Potential parameters in the force field for species unused in this work[S14,a]

Species	Atomic type	Charge (e^-)
framework P	P	2.625
Brønsted site (Si-O4(H3)-Al)	O4	-1.050
	H3	0.200
Lennard-Jones parameter		
Pair	A (eV $Å^{-12}$)	B (eV $Å^{-6}$)
Si ··· O4	218.1689	0.9583
Al ··· O4	1.0153	0.0005
O4 ··· O1	26877.9664	29.8306
O4 ··· O2	26877.9664	29.8306
O4 ··· O31	27097.4251	28.4516
O4 ··· O32	27097.4251	28.4516
O4 ··· O4	26877.9664	29.8306
P ··· O1	118.3529	0.093
P ··· O2	118.3529	0.093
P ··· O31	120.7430	0.0908
P ··· O32	120.7430	0.0908
P ··· O4	118.3529	0.093
P ··· Si	0.5403	0.0003
P ··· Al	0.9794	0.0004
P ··· P	0.5211	0.0003
Three-body parameter		
Three-body	k_ϑ (eV rad^{-2})	Θ_0 (°)
Oy – P– O*y*[b]	0.6998	109.470
P – O1 – Al	3.8604	139.689

[a] Si and Al are generic framework Si and Al, respectively, and labels for $SiO^-\cdots HOSi$ defects are the same as those in Table S15.
[b] O*y* is any oxygen with *y* = 1, 2, 31, and 32.

Table S21 Calculated shortest distances between F^- ions in 123TMP-containing zeolites as a representative sample (Table S6)

Zeolite	F atoms	F-F distance (Å)
123TMP-FER	F1-F4	5.85
	F2-F3	8.06
	F3-F2	8.06
	F4-F1	5.85
123TMP-ITE	F1-F4	8.46
	F2-F3	8.47
	F3-F6	4.44
	F4-F5	5.25
	F5-F4	5.25
	F6-F3	4.44
123TMP-ITW	F1-F2	9.12
	F2-F1	9.12
123TMP-PWO	F1-F3	5.48
	F2-F4	5.14
	F3-F1	5.48
	F4-F2	5.14
123TMP-PWW	F1-F3	5.56
	F2-F4	6.57
	F3-F1	5.56
	F4-F1	5.98
123TMP-RTH	F1-F3	5.31
	F2-F4	5.30
	F3-F1	5.31
	F4-F2	5.30

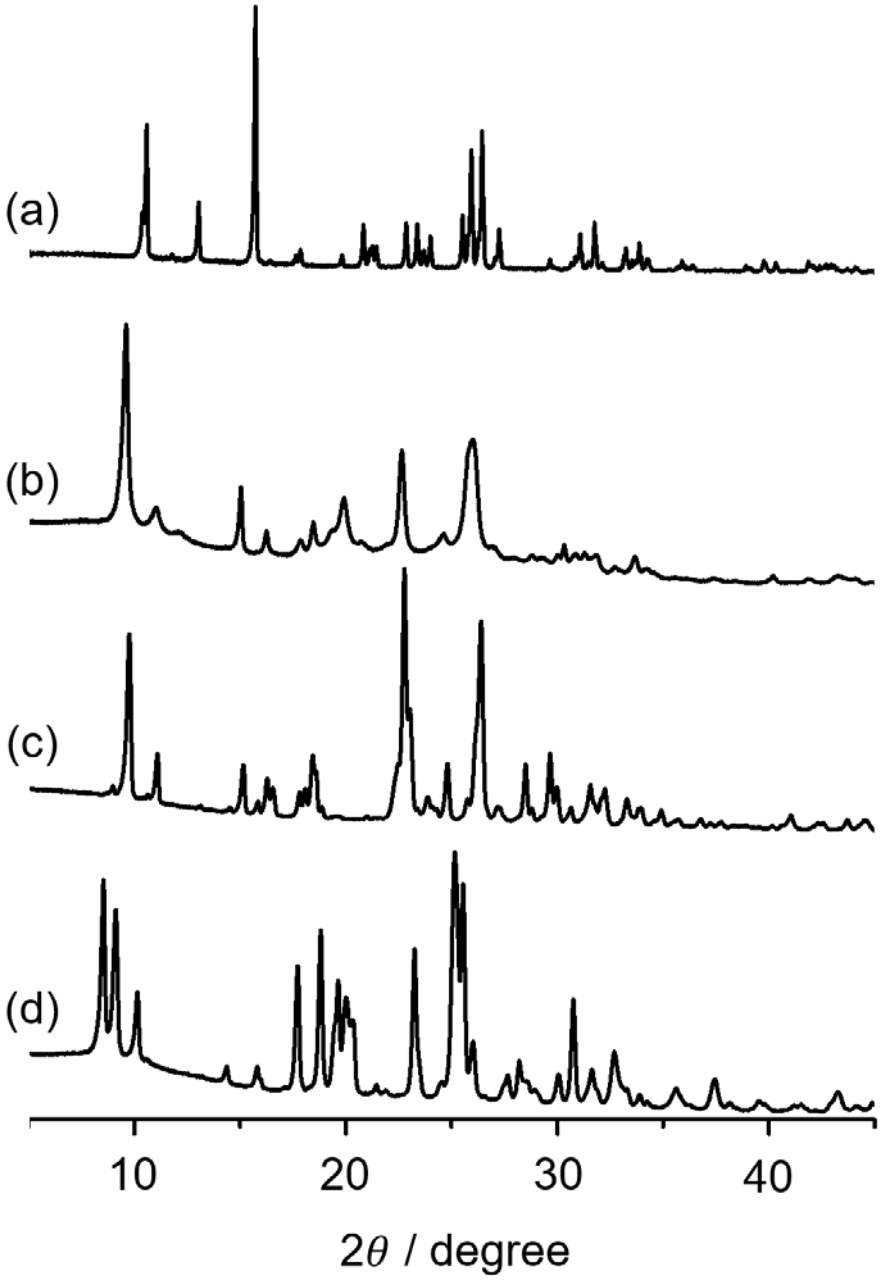

Fig. S1 PXRD patterns of the representative zeolites synthesized in this study: (a) 135TMP-ITW, (b) 134TMP-PWO, (c) 135TMP-PWW, and (d) 123TMP-RTH.

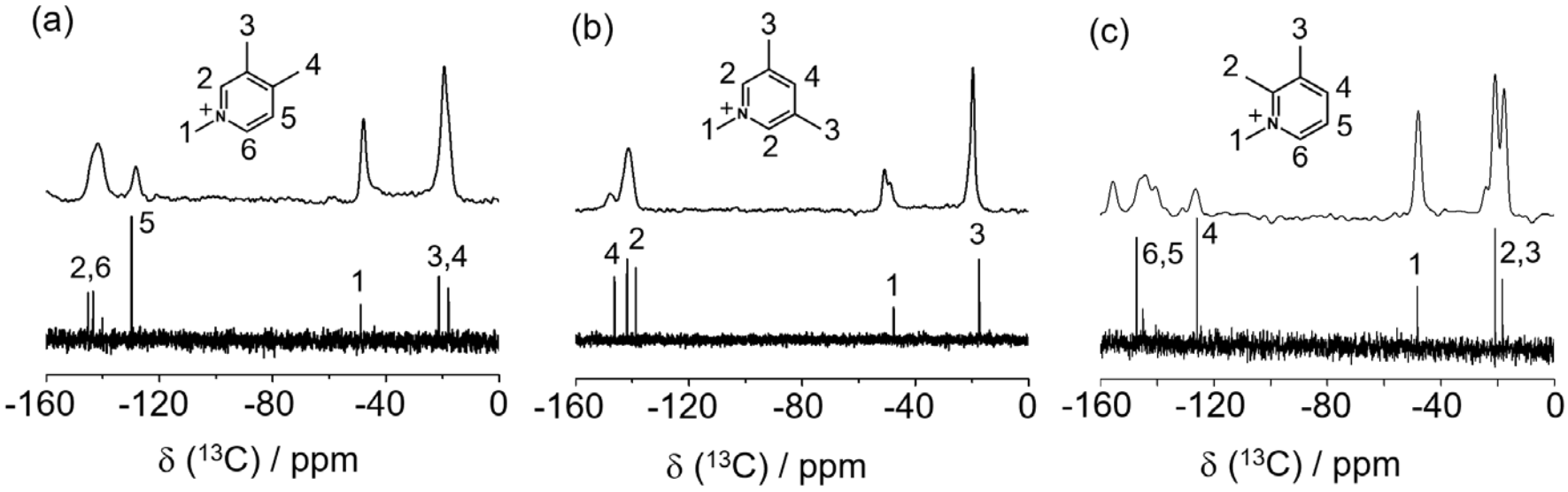

Fig. S2 (Top) ^{1}H-^{13}C CP MAS NMR spectra of as-synthesized (a) 134TMP-PWO, (b) 135TMP-PWW, and (c) 123TMP-RTH. The bottom traces are the solution ^{13}C NMR spectra of the iodide salt of 134TMP, 135TMP, and 123TMP in D_2O, showing the assignment of each resonance.

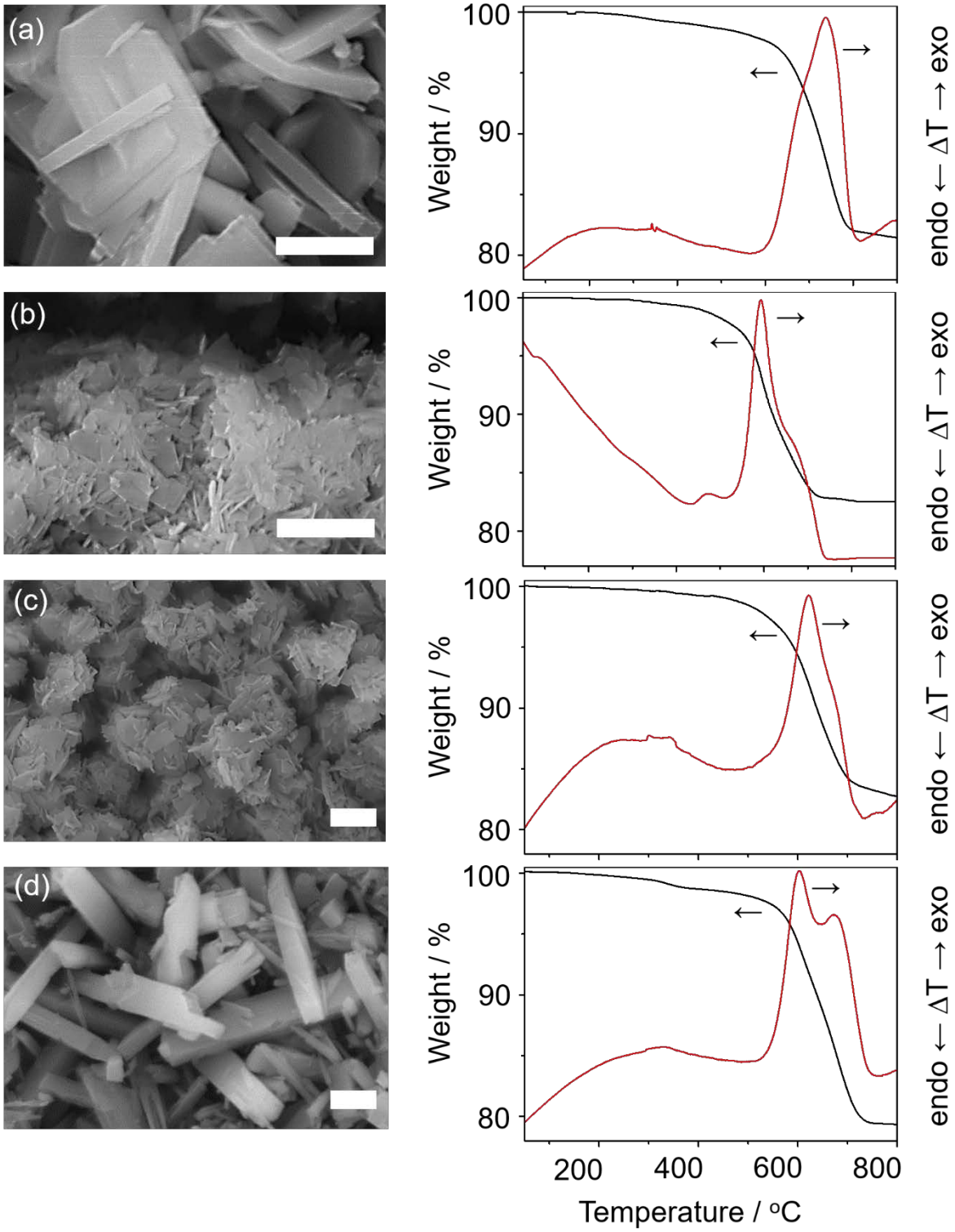

Fig. S3 SEM images (scale bar, 5 μm) and TGA/DTA profiles of as-synthesized (a) 135TMP-PWW, (b) 1234TMI-PWW, (c) 134TMP-PWO, and (d) 123TMP-RTH.

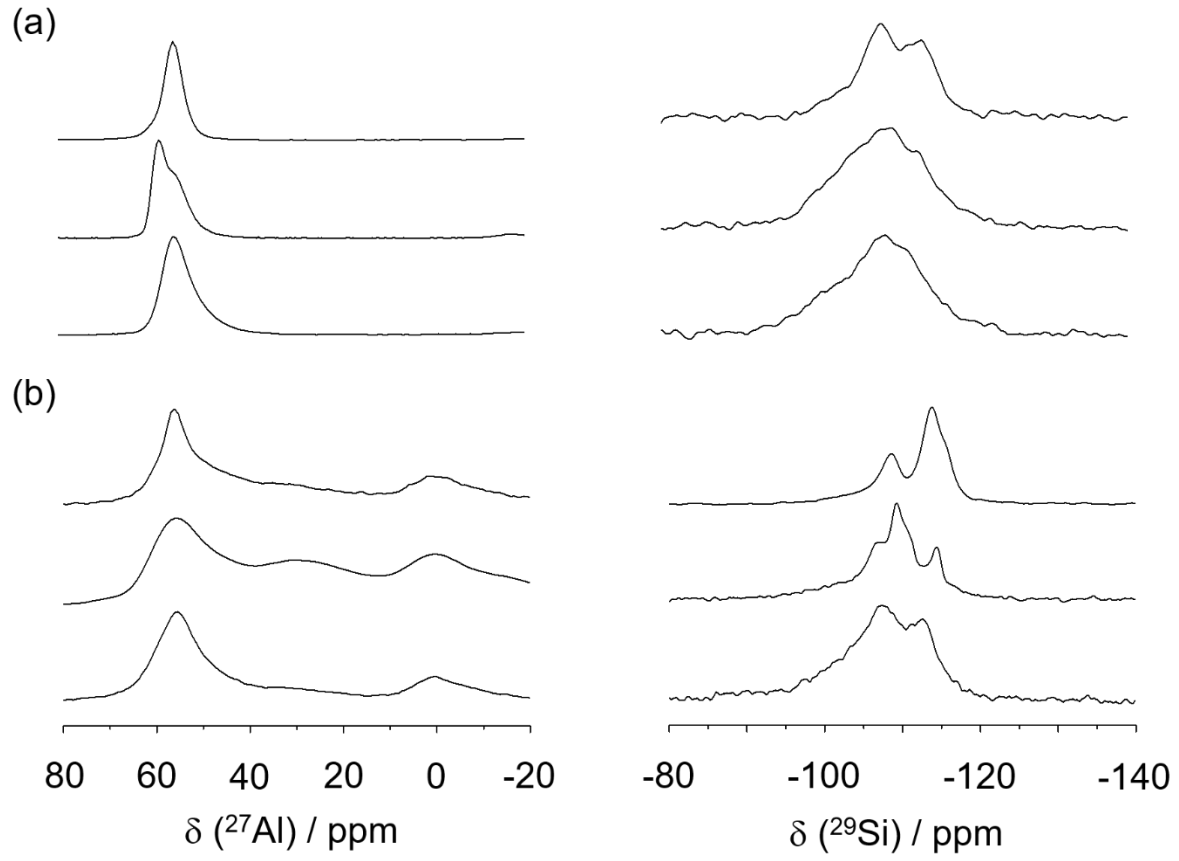

Fig. S4 ^{27}Al (left) and ^{29}Si (right) MAS NMR spectra of the (a) as-synthesized and (b) proton forms of (bottom to top) 134TMP-PWO, 135TMP-PWW, and 123TMP-RTH.

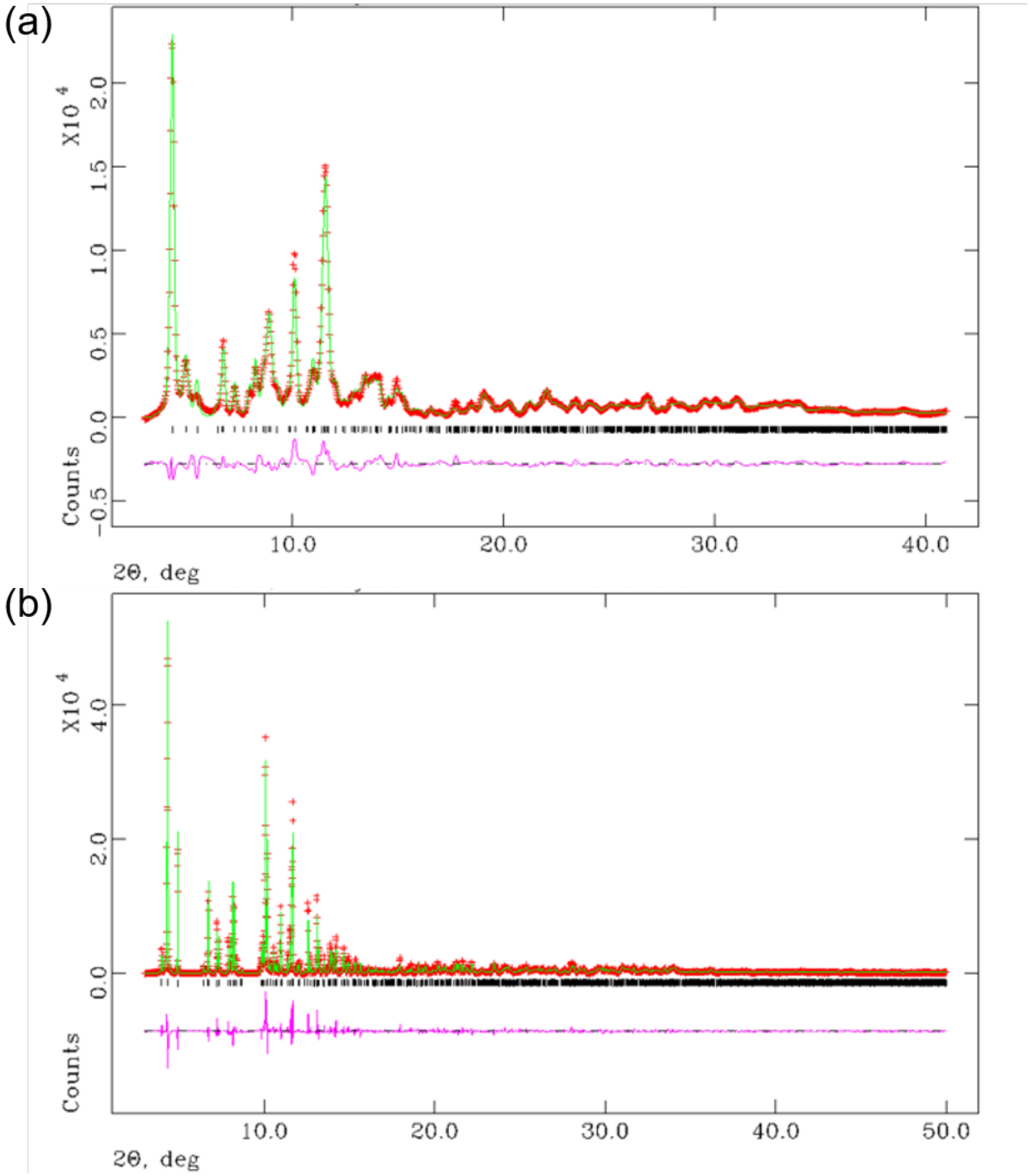

Fig. S5 Rietveld plots for as-synthesized (a) 134TMP-PWO and (b) 135TMP-PWW: observed data (+), calculated fit (solid line), and difference plot (lower trace). The tick marks represent the positions of allowed reflections.

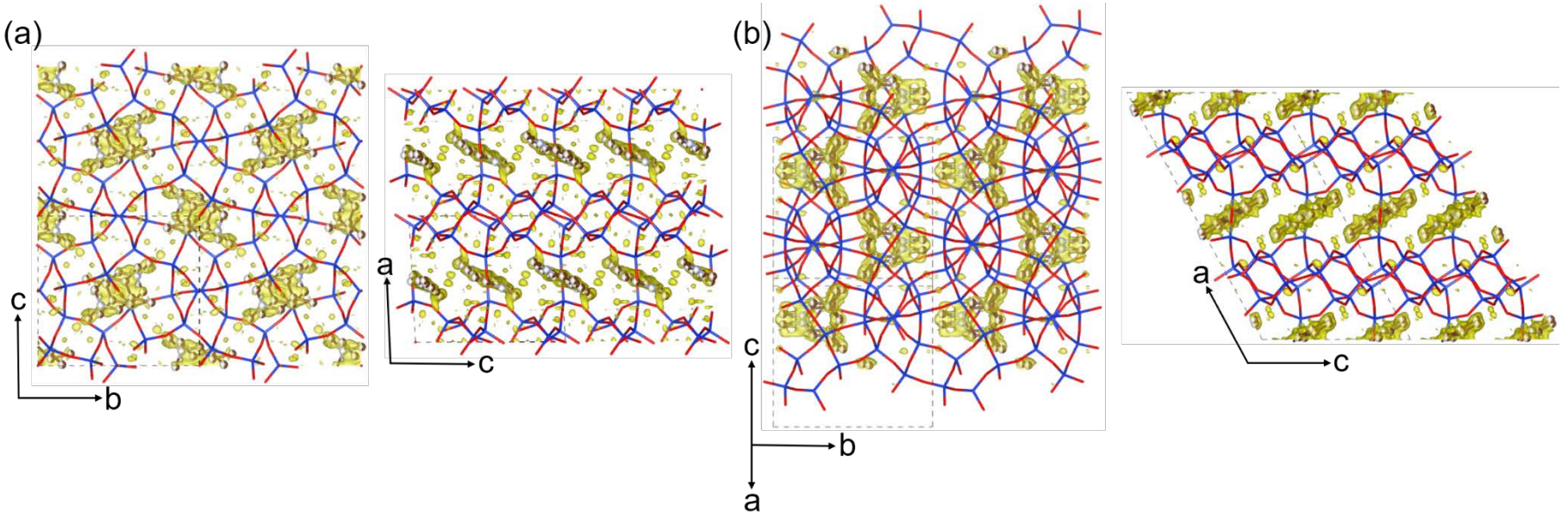

Fig. S6 Refined structures of as-synthesized (a) 134TMP-PWO and (b) 135TMP-PWW. The regions marked in translucent yellow indicate the positive difference electron density maps visualized using the whole data set, after refining the framework atoms only against the high-angle (*d*-space < 2.0 Å) data. Color code: Si, blue; O, red; C, brown; and N, pale blue.

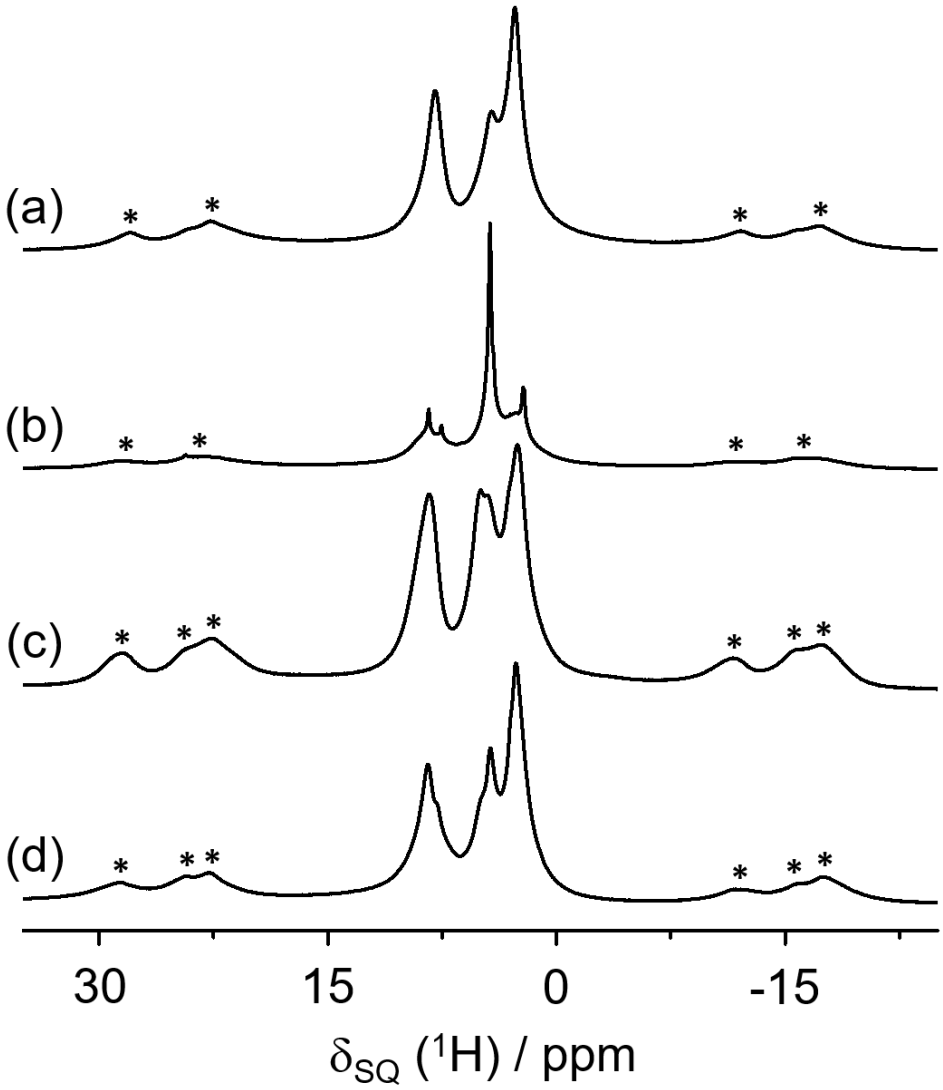

Fig. S7 ^{1}H MAS NMR spectra of as-synthesized (a) 135TMP-ITW, (b) 134TMP-PWO, (c) 135TMP-PWW, and (d) 123TMP-RTH. Spinning sidebands are marked by asterisks.

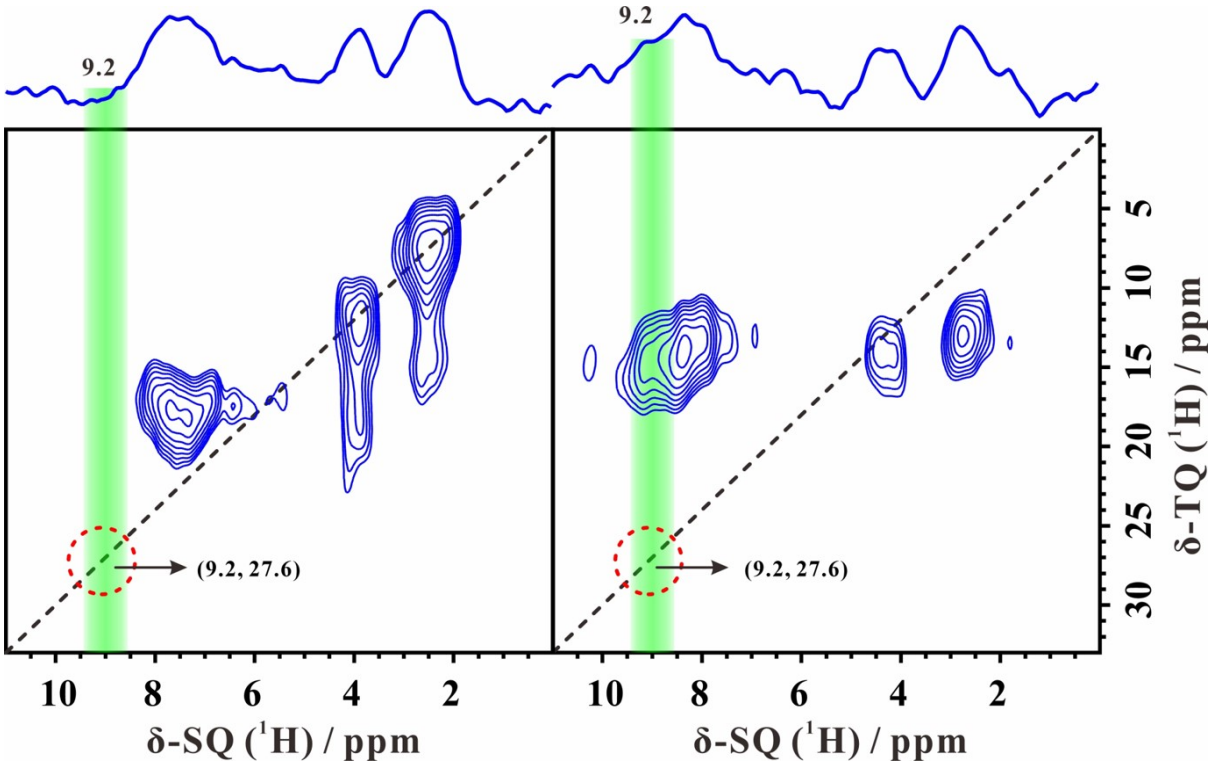

Fig. S8 ^{1}H TQ-SQ MAS NMR spectra of as-synthesized (left) 134TMP-PWO and (right) 135TMP-PWW. The absence of a ^{1}H TQ-SQ autocorrelation signal at 27.6 ppm (3 × 9.2 ppm) indicates that their defects may be considered as a $1SiO^{-}$ 2SiOH cluster rather than as a $1SiO^{-}$ 3SiOH one (see main text Fig. 3).

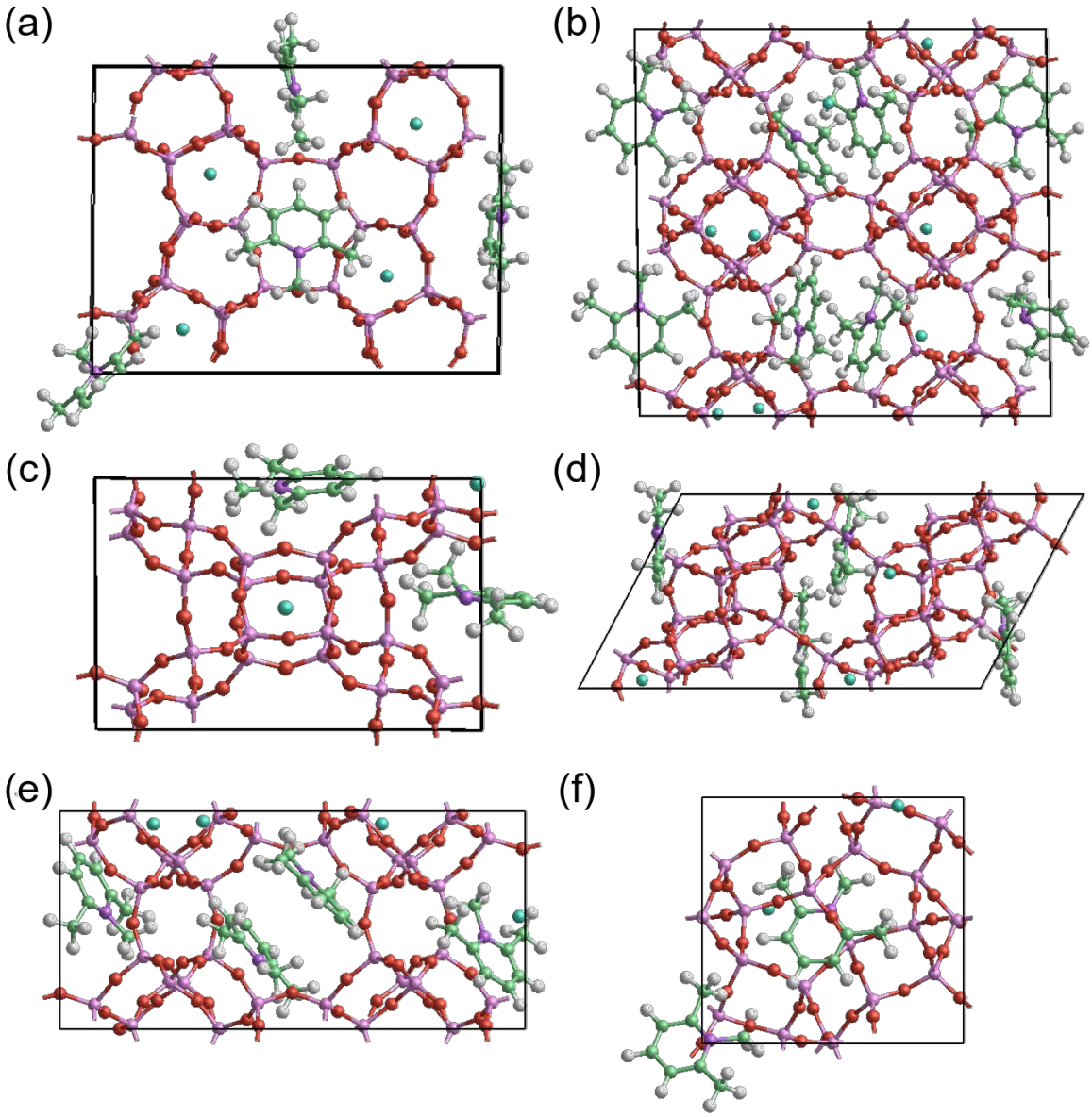

Fig. S9 Unit cell representations of pure-silica (a) 126TMP-FER, (b) 126TMP-ITE, (c) 126TMP-ITW, (d) 126TMP-PWW, (e) 126TMP-RTH, and (f) 126TMP-PWO. Color code: Si, pink; O, red; C, green; N, purple; H, grey; F, cyan.

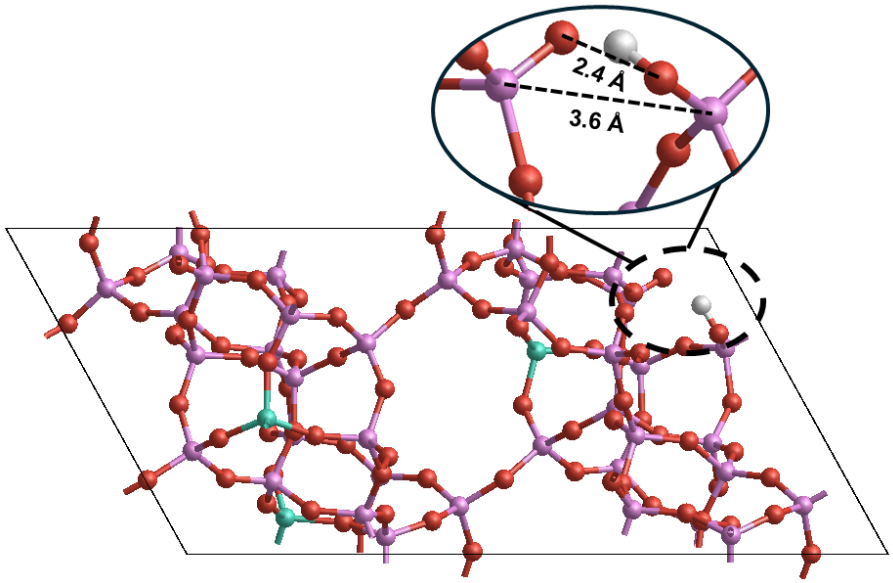

Fig. S10 Representation of the 1:1 connectivity defect generated in the PWW framework model. The O···O distance between SiO^- and SiOH groups is 2.40 Å. Color code: Si, pink; O, red; H, white; Al, turquoise.

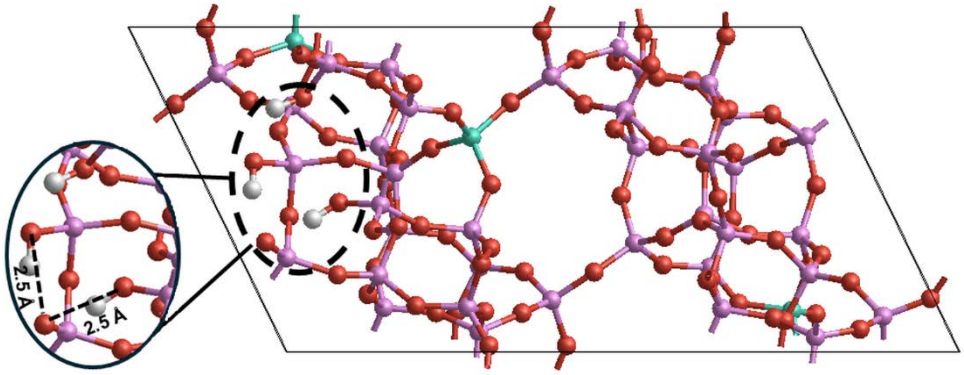

Fig. S11 Representation of the 2:1 connectivity defect generated in the PWW framework model. The average O···O distance between SiO^- and SiOH groups is 2.50 Å. Color code: Si, pink; O, red; H, white; Al, turquoise.

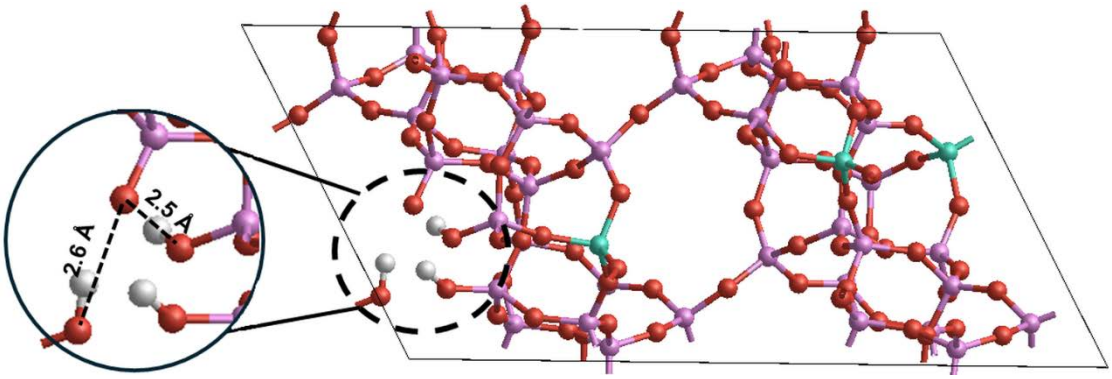

Fig. S12 Representation of the 3:1 vacancy defect generated in the PWW framework model. The average O···O distance between SiO^- and SiOH groups is 2.55 Å. Color code: Si, pink; O, red; H, white; Al, turquoise.

REFERENCES

S1. D. Jo, G. T. Park, J. Shin and S. B. Hong, A Zeolite Family Nonjointly Built from the 1,3-Stellated Cubic Building Unit, *Angew. Chem. Int. Ed.*, 2018, **57**, 2199-2203.

S2. H. M. Rietveld, A Profile Refinement Method for Nuclear and Magnetic Structures, *J. Appl. Cryst.*, 1969, **2**, 65–71.

S3. A. Le Bail, H. Duroy and J. L. Fourquet, Ab-Initio Structure Determination of $LiSbWO_6$ by X-Ray Powder Diffraction, *Mater. Res. Bull.*, 1998, **23**, 447–452.

S4. B. H. Toby, EXPGUI, a Graphical User Interface for GSAS, *J. Appl. Crystallogr.*, 2001, **34**, 210–213.

S5. A. C. Larson and R. B. Von Dreele, *General Structure Analysis System (GSAS)*, Los Alamos National Laboratory Report LAUR, 86–748, 2004.

S6. C. H. Lake and B. H. Toby, Rigid Body Refinements in GSAS/EXPGUI, *Powder Diffr.*, 2001, **26**, S13–S21.

S7. M. Gálvez-Llompart, A. Cantín, F. Rey and G. Sastre, Computational Screening of Structure Directing Agents for the Synthesis of Zeolites. A Simplified Model, *Z. Kristallogr.I*, 2019, **234**, 451-460.

S8. J. D. Gale, GULP: A Computer Program for the Symmetry-Adapted Simulation of Solids, *J. Chem. Soc., Faraday Trans.*, 1997, **93**, 629-637.

S9. T. Lemishko, S. Valencia, F. Rey, M. Jiménez-Ruiz and G. Sastre, Inelastic Neutron Scattering Study on the Location of Brønsted Acid Sites in High Silica LTA Zeolite, *J. Phys. Chem. C*, 2016, **120**, 24904-24909.

S10. G. Brunklaus, H. Koller and S. I. Zones, Defect Models of As-Made High-Silica Zeolites: Clusters of Hydrogen-Bonds and Their Interaction with the Organic Structure-Directing Agents Determined from ^{1}H Double and Triple Quantum NMR Spectroscopy, *Angew. Chem. Int. Ed.*, 2016, **55**, 14459-14463.

S11. S. J. Clark, M. D. Segall, C. J. Pickard, P. J. Hasnip, M. I. J. Probert, K. Refson and M. Payne, First principles methods using CASTEP, *Z. Kristallogr. Cryst. Mater.*, 2009, **220**, 567-570.

S12. Ö. F. Altundal, S. Leon and G. Sastre, Different Zeolite Phases Obtained with the Same Organic Structure Directing Agent in the Presence and Absence of Aluminum: The Directing Role of Aluminum in the Synthesis of Zeolites, *J. Phys. Chem. C*, 2023, **127**, 10797-10805.

S13. Ö. F. Altundal and G. Sastre, The Directing Role of Aluminum in the Synthesis of PST-21 (PWO), PST-22 (PWW), and ERS-7 (ESV) Zeolites, *J. Phys. Chem. C*, 2023, **127**, 15648-15656.

S14. A. Misturini, F. Rey and G. Sastre, Molecular Simulation of Biobutanol Recovery Using LTA and CHA Zeolite Nanosheets with an External Surface, *J. Phys. Chem. C*, 2022, **126**, 17680-17691.

S15. K.-P. Schröder, J. Sauer, M. Leslie, C. R. A. Catlow and J. M. Thomas, Bridging Hydroxyl Groups in Zeolitic Catalysts: A Computer Simulation of Their Structure, Vibrational Properties and Acidity in Protonated Faujasites (HY Zeolites), *Chem. Phys. Lett.*, 1992, **188**, 320-325.